Behav Res (2014) 46:396–405
DOI 10.3758/s13428-013-0371-9

Development of a simple pressure and heat stimulator for intra- and interdigit functional magnetic resonance imaging

Hyung-Sik Kim · Mi-Hyun Choi · Hyun-Joo Kim · Sang-Pyo Hong · Jang-Yeon Park · Jae-Hoon Jun · Jeong-Han Yi · Yoon-Gi Chung · Sung-Phil Kim · Jong-Rak Park · Dae-Woon Lim · Soon-Cheol Chung

Published online: 17 July 2013

Abstract For this study, we developed a simple pressure and heat stimulator that can quantitatively control pressure and provide heat stimulation to intra- and interdigit areas. The developed stimulator consists of a control unit, drive units, and tactors. The control unit controls the stimulation parameters, such as stimulation types, intensity, time, and channel, and transmits a created signal of stimulation to the drive units. The drive units operate pressure and heat tactors in response to commands from the control unit. The pressure and heat tactors can display various stimulation intensities quantitatively, apply stimulation continuously, and adjust the stimulation areas. Additionally, they can easily be attached to and detached from the digits. The developed pressure and heat stimulator is small in total size, easy to install, and inexpensive to manufacture. The new stimulator operated stably in a magnetic resonance imaging (MRI) environment without affecting the obtained images. A preliminary functional magnetic resonance imaging (fMRI) experiment confirmed that differences in activation of somatosensory areas were induced from the pressure and heat stimulation. The developed pressure and heat stimulator is expected to be utilized for future intra- and interdigit fMRI studies on pressure and heat stimulation.

Keywords Pressure stimulator · Heat stimulator · Intradigit · Interdigit · fMRI

H.-S. Kim · M.-H. Choi · H.-J. Kim · S.-P. Hong · J.-Y. Park · J.-H. Jun · J.-H. Yi · S.-C. Chung
Department of Biomedical Engineering, Research Institute of Biomedical Engineering, College of Biomedical & Health Science, Konkuk University, Chungju, South Korea

Y.-G. Chung · S.-P. Kim
Department of Brain and Cognitive Engineering, Korea University, Seoul, South Korea

J.-R. Park
Department of Photonic Engineering, Chosun University, Gwangju, South Korea

D.-W. Lim
Department of Information & Communication Engineering, Dongguk University, Seoul, South Korea

S.-C. Chung (✉)
Department of Biomedical Engineering, Research Institute of Biomedical Engineering, College of Biomedical & Health Science, Konkuk University, 268 Chungwon-daero, Chungju-si, Chungcheongbuk-do 380-701, South Korea
e-mail: scchung@kku.ac.kr

Many studies have been performed to identify the characteristics of perception and cognition in tactile sensation, which has been induced by touch or pressure and warm or pain sensations due to heat stimulation using functional magnetic resonance imaging (fMRI).

In an MR environment, several techniques, including pneumatic (Briggs et al., 2004; Chakravarty, Broadbent, Rosa-Neto, Lambert, & Collins, 2009; Gallasch et al., 2010; Montant, Romaiquere, & Roll, 2009; Wienbruch, Candia, Svensson, Kleiser, & Kollias, 2006), shaft (Golaszewski et al., 2002), piezoceramic (Gizewski et al., 2005; Harrington, Wright, & Downs, 2000), and electromagnetic (Graham, Staines, Nelson, Plewes, & McIlory, 2001) approaches, have been used for vibrotactile stimulation. fMRI studies using these methods were also reported with stimulation on various parts of the body, such as the hands, face, arms, and legs (Bleton et al., 2011; Geyer et al., 2001; Roiha et al., 2011; Tsekos, Khanicheh, Christoforou, & Mavroidis, 2007). Among the methods used for vibrotactile stimulation, the piezoceramic and electromagnetic approaches especially have the advantages of easy control of

tactor size as well as quantitative control of the stimulation parameters. Accordingly, they facilitate brain mapping as well as the analysis of brain function in the case of intra- and interdigit stimulation (Graham et al., 2001; Hegner et al., 2007; Schweisfurth, Schweizer, & Frahm, 2011; Van Westen et al., 2004). It has been reported that the activation region of somatosensory area I became larger with an increase in the intensity of vibrotactile stimulation on the index finger (Graham et al., 2001). It has also been reported that, when a vibrotactile stimulus was presented to the fingertip and the base of the index and little fingers, the activated patterns in the brain depended on finger type, showing an evident intradigit somatotopic arrangement in the case of the little finger (Schweisfurth et al., 2011).

However, few fMRI studies have been reported on intra- and interdigit stimulation with pressure or heat, due to some technical limitations of the existing stimulators. Conventional stimulators with MR compatibility use air puffs (Huang & Sereno, 2007; Overduin & Servos, 2004), a diaphragm (Hlushchuk & Hari, 2006; Hlushchuk, Forss, & Gari, 2004; Mottonen, Jarvelainen, Sams, & Hari, 2004), and a von Frey filament (Dresel et al., 2008; Habre-Hallage et al., 2010) for pressure stimulation. Although the air-puff technique, in which compressed air is blown directly on the skin, has several benefits, such as MR compatibility, capability of strong stimulation intensity, and the ability to stimulate any part of the body, it can have a difficulty in controlling the stimulation intensity continuously (Gassert et al., 2006). Furthermore, the stimulated area to which the compressed air is blown typically generates an additional tactile sensation of slight cooling (Huang & Sereno, 2007). Especially, because it is not easy to have a fine and precise control of stimulating the targeted area, the air-puff method can hardly be used for intradigit fMRI study. In contrast, the diaphragm technique—in which compressed air is blown into a diaphragm, not directly on the skin—can control the stimulated area. However, since it cannot provide a wide range of stimulation intensity (e.g., strong stimulation intensity) in a continuous way, it is not desirable for an fMRI study that would require fine control of stimulation intensity (Mertens & Lutkenhoner, 2000). Both the air-puff and diaphragm methods have another disadvantage, in that they require a large-sized system with careful use, because they require an air compressor and an air tank as well. The von Frey filament method can deliver stimulation to a very small targeted area ($\leq$1 mm^2) with precise control of intensity, and thus has mainly been used for quantitative sensory testing studies (Dresel et al., 2008). With this method, however, only specific, point-like stimulation is available, and the stimulated area needs to be modified to change the stimulation intensity, which is not appropriate for an intra- and interdigit fMRI study.

Regarding heat stimulators, the Peltier Thermode (Becerra et al., 1999; Kubina et al., 2010; Peltz et al., 2011) and a light bulb (Zhang et al., 2003) are mainly used for heat stimulation. The Peltier Thermode (Medoc Advanced Medical Systems, Ramat Yishai, Israel) method can hardly be used for an intra- and interdigit fMRI study, because it requires a large and expensive tactor. On the other hand, the light bulb method is simple, easy to use, and inexpensive, because it offers heat stimulation by using the heat radiated from a high-power lamp. However, this method is not appropriate for an fMRI study that would require accurate control of stimulation, because the reflectance of light from the skin makes it difficult to control temperature with accuracy and to deliver uniform heat to a targeted area (Arendt-Nielsen & Chen, 2003).

Conventional stimulators for pressure or heat stimulation can also have a limitation in their use for some brain-mapping research that requires a more precise experimental design—for example, an intra- and interdigit fMRI study designed for identifying somatotopic arrangement. Besides, they need to be improved in terms of system size, manufacturing cost, and ease of use.

In this study, we developed a simple stimulator that can present quantitatively and precisely controllable pressure and heat stimulations for intra- and interdigit fMRI studies, which is expected to overcome the technical weaknesses of existing stimulators.

Method

Figure 1 shows the overall configuration of the pressure and heat stimulator we developed. The stimulator consists of a control unit, pressure and heat drive units, and pressure and heat tactors. The control unit and pressure drive unit are positioned outside an MR shield room, whereas the heat drive unit and tactors are positioned inside the room.

Control unit

The control unit selects pressure and heat stimulation and controls stimulation parameters including intensity, time, and channel of stimulation. Also, it enables synchronization with the MR system. The control unit uses an AVR-family ATMEGA 128 controller (Atmel, San Jose, CA, USA), which is a general-purpose eight-bit microcontroller. This controller works at a 4.5- to ~5.5-V operating voltage, and it has several capabilities, such as an eight-channel, ten-bit analog-to-digital converter (ADC) and eight-bit and 16-bit timer/counters.

The pressure stimulus is controlled by controlling a rolling pump using the duty rate of pulse width modulation (PWM) regulated by the microcontroller's timer/counter. Stimulation can be presented at 17 levels (0 to ~8.5 psi) of intensity, three channels, and over a time scale of seconds.

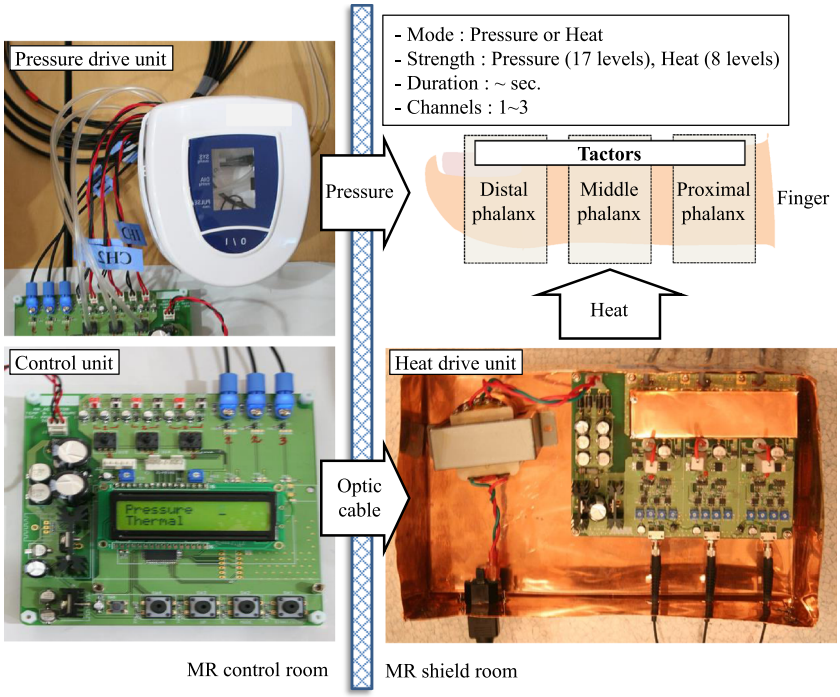

Fig. 1 Overall configuration of a simple MR-compatible pressure and heat stimulator

The heat stimulus can be controlled with the use of a 12-bit quad-channel digital-to-analog converter (DAC; Model DAC7554, Texas Instruments, Dallas, TX) regulated by the serial peripheral interface (SPI) function of a microcontroller. The control (baseline) temperature can be set at four levels (30 °C to ~33 °C). Stimulation temperature is controllable at eight levels (42 °C to ~49 °C), and stimulation can be presented for seconds and over three channels. An electric signal is converted into an optical signal by using a light-emitting diode (LED) driving circuit whose brightness is regulated via the amplitude of the stimulation signal, and the optical stimulation signal is transferred to the heat drive unit inside the MR shield room by using an optic cable (Fig. 2).

The user can input stimulation parameters using buttons on the control unit and can monitor performance and status with a character liquid crystal display (LCD; see Fig. 1). Also, the stimulation parameters can be controlled with E-Prime software (Psychology Software Tools, Sharpsburg, PA) by a PC. E-Prime is a well-known software package that is used as a visual and auditory stimulation tool in psychology, neuroscience, and cognitive and behavioral sciences (Ho & Spence, 2007). Therefore, tactile, auditory, and visual

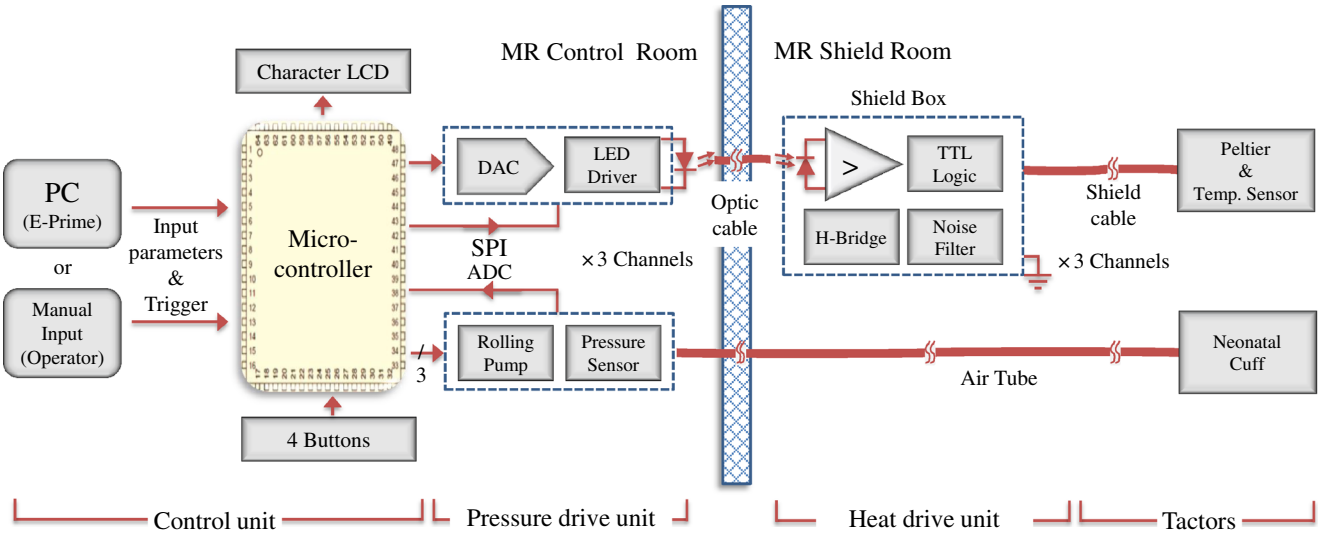

Fig. 2 Block diagram of the MR-compatible pressure and heat stimulator

stimulation can be generated simultaneously using the software (Kim et al., 2011). Stimulation parameters are delivered to the control unit through the LPT-1 port in a PC.

Drive units

The drive units operate the pressure and heat tactors in response to commands from the control unit. The pressure drive unit, which is located outside the MR shield room, uses a rolling pump (OKENSEIKO, Tokyo, Japan) and a 7-m-long air tube to send the air to the pressure tactor positioned inside the MR shield room. This configuration does not need any protective device to minimize the mutual interference effects with the MR scanner. The pressure stimulation is delivered by emitting air through the use of a solenoid switch. Because a rolling pump is connected to each of the three channels, each channel can be controlled independently. The intensity of the pressure stimulation generated can be measured using a Model 33A-010G-2210 pressure sensor (Sensormate Enterprise, Chang Hua, Taiwan) and fed back to the microcontroller, which uses feedback signals from the pressure sensor to regulate the pressure precisely in real time (Fig. 2).

Heat stimulation uses heat generated from a Peltier element. The heat drive unit should be located inside the MR shield room in order to provide current to the Peltier element. For this reason, it should be galvanically isolated from the control unit. In addition, a special protective device is needed to minimize interaction with the MR system. An optical signal from the control unit is converted into an electric signal using a photodiode, and this generates signals to operate an H-bridge circuit according to the values of the comparator and transistor–transistor logic. The current generated from the H-bridge is delivered to the Peltier element after passing through a noise filter (Fig. 2). The noise filter can protect the heat drive unit from induced current by radio frequency (RF) and gradient pulse during the acquisition of MR images. Figure 3 shows the schematic of the noise filter, which consists of a LC resonator with an inductor (represented by the letter L) and a capacitor (represented by the letter C). Due to the connection of the Peltier element to each of the three channels, each channel can be controlled independently.

Tactors

Figure 4 shows the appearance of the pressure and heat tactors and a schematic diagram of the tactors positioned on a finger. The pressure tactor offers pressure stimulus on each phalanx of a finger using a neonatal cuff designed for measuring noninvasive blood pressure of a newborn infant. Because it is made of vinyl and Velcro tape and is available in several models with different lengths, it can easily be attached on and detached from fingers and compensate for differences in finger circumference (Fig. 4a).

The heat tactor, which is a Peltier element made of ceramic, is able to present heat stimulus once it is fixed on each phalanx of a finger by using Velcro tape. A shield cable is used to supply current from the heat drive unit. The intensity of the heat stimulation is measured by using an LM35 precision centigrade temperature sensor (National Semiconductor, Santa Clara, CA) attached to the heat tactor and a comparator that receives a feedback signal to control the driving current of the H-bridge, consequently making it possible to regulate temperature. The LM35 temperature sensor, made of a TO-92 plastic package, is attached to the center of the Peltier element (Fig. 4b).

MRI testing

Since the pressure tactor is composed of nonmetallic materials, it can be used in the MR environment without limits. However, the Peltier element of the heat tactor is composed of metallic materials that may have a mutual interference effect with the MR system. Therefore, effects on an MR image were analyzed while changing operating conditions of the heat tactor. The three following conditions were compared by means of the acquired MR images: no heat tactors (without heat tactors), heat tactors positioned 30 cm away from the center of the head coil and not operated (with heat tactors), and heat tactors operated in the same position (with heat tactors + operation). The single-shot gradient echoplanar imaging (EPI) of a cylindrical phantom

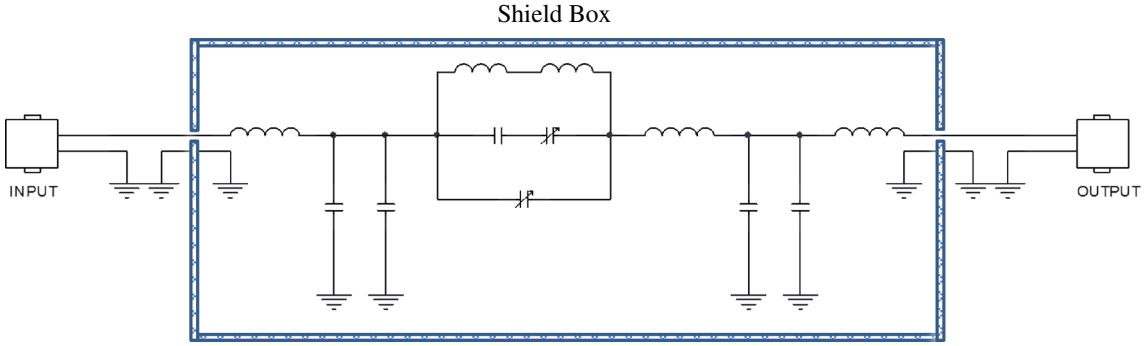

Fig. 3 Schematic of the noise filter

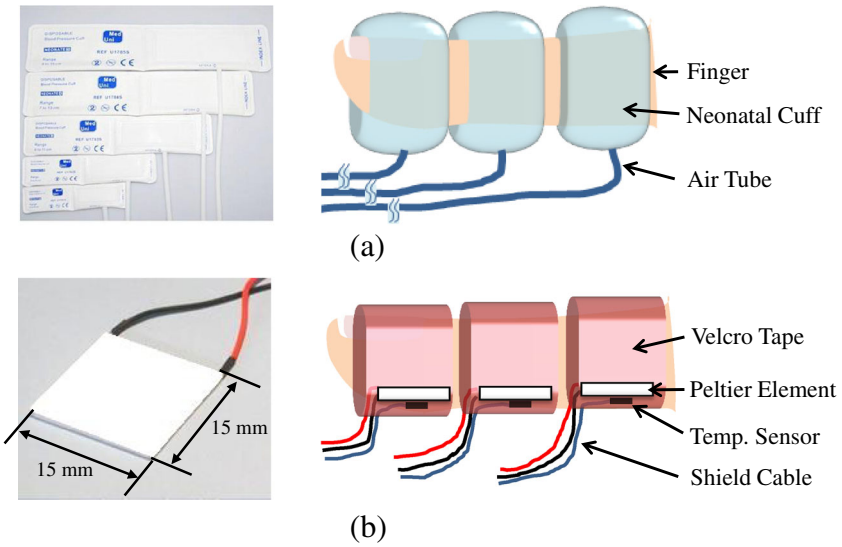

Fig. 4 Appearance of the pressure (**a**) and heat (**b**) tactors and schematic diagrams of the tactors put on a finger

with a 3.0-T MAGNETOM Trio MR scanner (Siemens Healthcare, Munich, Germany) were collected with the following parameters: repetition time/echo time = 3,000/30 ms, field of view = 192 mm, matrix size = 128 × 128, slice thickness = 2 mm, number of axial slices = 35, and flip angle = 90.

Next, the operating status of the pressure and heat tactors placed on fingers was monitored while acquiring the EPI data with the use of selected image parameters from the experiment above. To monitor the operating status of the pressure tactor, experiments were conducted at under 4.5 psi and at 8.5 psi (max level). To monitor the operating status of the heat tactor, experiments were conducted at stimulation temperatures of 42 °C and 49 °C (max), with a baseline temperature of 33 °C.

fMRI experiments

Preliminary fMRI experiments were carried out using the developed pressure and heat stimulator. Five male (24.8 ± 4.1 years) college students participated. All of the subjects were right-handed, and none reported having a history of psychiatric or neurological disorders. The overall procedure was explained to all subjects who provided informed consent for the procedure. We used the same imaging parameters as in the phantom image experiments.

Figure 5 shows the paradigm for the fMRI experiments. One block in the pressure stimulation experiment consisted of a 30-s-long rest (0 psi) and a 30-s-long stimulation (8.5 psi) phase, and these phases were repeated three times. One block in the heat stimulation experiment consisted of a 78-s-long rest (33 °C) and a 39-s-long stimulation (42 °C) phase. These phases were repeated three times, considering the rising and falling times of the heat tactors. An experiment was conducted targeting the distal phalanges of the index finger and little finger of the right hand. We changed the position of the tactor and marked a stimulated region of the finger in order to deliver pressure and heat stimuli to the same location. All of the subjects participated in four experiments (two types of stimulation on two fingers). All subjects closed their eyes and wore a headset in order to block surrounding disturbances.

The fMRI data were analyzed with SPM 8 (Wellcome Department of Cognitive Neurology, London, UK). All functional images were aligned with the anatomic images of the study by using the affine transformation routines built into SPM 8. The realigned scans were co-registered to the participant's anatomic images obtained within each session and normalized to SPM 8's template image. Motion correction was done using sync interpolation. The time-series data

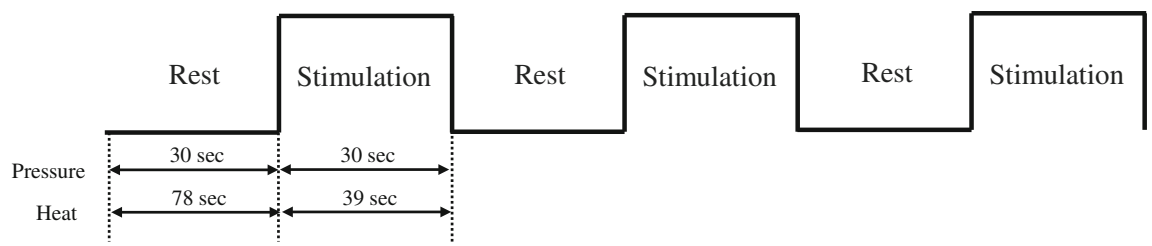

Fig. 5 Block design of the fMRI experiments

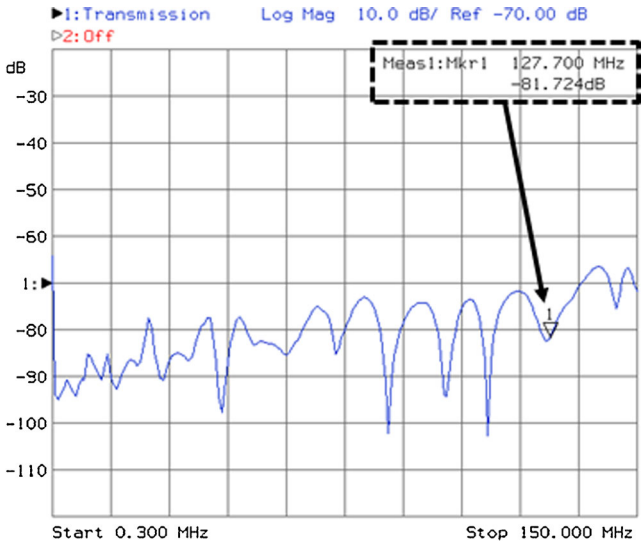

Fig. 6 Performance of the noise filter

were filtered with a 180-s high-pass filter to remove artifacts due to cardiorespiratory and other cyclical influences. The functional map was smoothed with a 7-mm isotropic Gaussian kernel prior to statistical analysis. Statistical analyses were done both individually and at a group level using the general linear model and the theory of Gaussian random fields implemented in SPM 8. Using the subtraction procedure, activated areas between the rest and stimulation phases were color-coded using the *t* score.

In the case of the heat stimulation, only images obtained for 30 s in the stimulation phase of each block, after the initial 9 s of the block, were used for the analysis, in consideration of the rising time of the heat tactors. This is because heat stimulation reaches the desired value only after a period of rising time after the heat tactor is turned on. The rising time of the heat tactor was about 7 s. For an accurate analysis, the falling time of the heat tactor and the effect of residual heat on the finger also needed to be taken into account. The falling time of the heat tactor was about 10 s. Considering the falling time of the heat tactors and the effect of residual heat, only images obtained over 30 s in the rest phase of each block, following the initial 48 s, were used for the analysis. In the case of the pressure stimulation, however, all of the images obtained were used for analysis, because the rising and falling times of the pressure tactor were relatively short in each phase—that is, 3.5 and 0.2 s, respectively—and there was no effect of residual pressure, unlike in heat stimulation, during which residual heat remained when the tactor was no longer activated. Hence, the same duration of rest and stimulation times, both of which were set to be 30 s, were used for both cases of pressure and heat stimulations.

Results

Figure 6 shows the performance of the noise filter to protect the heat drive unit. We could protect the drive unit by attenuating the induced current from the RF and gradient pulses of the MR scanner below −60 dB. As is shown in Fig. 6, the attenuating signals from input to output satisfied the threshold of −60 dB in the range from 0.3 to ~150 MHz. Specifically, the attenuation was measured to be −81.7 dB at 127.7 MHz, which is the Larmor frequency of a hydrogen proton in a 3-T MR scanner. Thus, the developed heat stimulator could be used without compensation for all MR scanners below 3.0 T. The performance of the noise filter was measured with an RF network analyzer, 8712ET (Agilent Technologies, Santa Clara, CA).

Figure 7 shows the results of the single-shot gradient EPI from the condition in which the heat tactors were operated (i.e., heat tactors + operation). Slice B is the middle axial image, and Slices A and C are the axial images 26 mm above and below Slice B, respectively. As is shown in Fig. 7, the signal-to-noise ratio (SNR) was calculated for three cases—without heat tactors, with heat tactors, and with heat tactors + operation—by dividing each intensity of three regions (Locations 1–3 [L1–L3 in Table 1]) by the average intensity of four background regions (N1, N2, N3, and N4). Table 1 shows the SNRs of the EPI for three cases (without

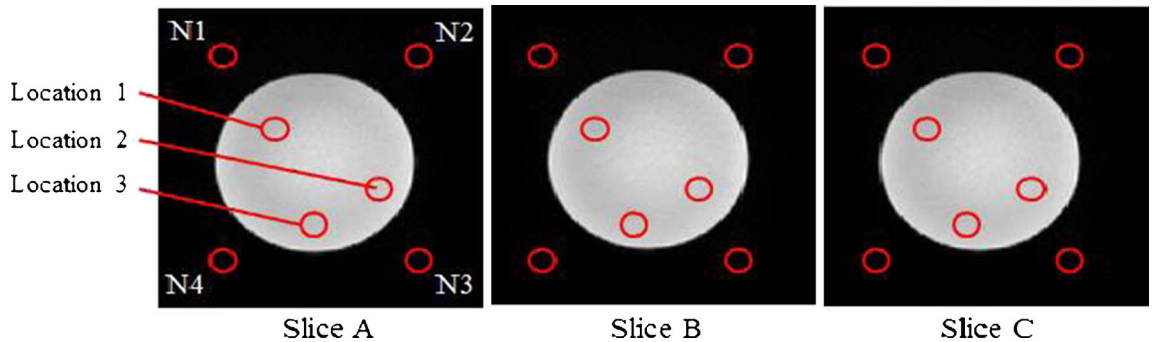

Fig. 7 Echoplanar imaging of a water phantom obtained when activating heat tactors (with heat tactors + operation). Slice A, 26 mm above Slice B; Slice B, middle axial image; Slice C, 26 mm below Slice B. Locations 1, 2, and 3 are regions of interest, and N1, N2, N3, and N4 are background regions

Table 1 Signal-to-noise ratios of magnetic resonance images for three cases (i.e., without heat tactors, with heat tactors, and with heat tactors + operation) of three slices (A, B, and C) at three regions (L1, L2, and L3)

	Slice A				Slice B				Slice C			
	L1	L2	L3	Avg.	L1	L2	L3	Avg.	L1	L2	L3	Avg.
Without heat tactors	186.0	210.3	199.0	198.4	182.0	207.1	192.9	194.0	174.5	207.1	203.4	195.0
With heat tactors	194.7	216.6	205.0	205.4	184.3	207.0	195.0	195.4	174.0	207.0	203.0	194.7
With heat tactors + operation	186.6	210.1	199.0	198.6	181.2	206.3	193.0	193.5	172.8	205.4	200.7	193.0

heat tactors, with heat tactors, and with heat tactors + operation). As can be seen in Table 1, the differences in SNRs were very small and, as is shown in Fig. 7, there was no distortion of the MR image when the heat tactors were operated. Thus, we could confirm that the heat stimulator did not affect the MR images.

Figure 8 shows the pressure and heat tactors placed on the fingers. Additionally, this figure shows the output signals of the pressure sensor and the temperature sensor regarding two stimulation intensities measured while obtaining the MR images simultaneously. The tactors were not limited by the circumference of a finger, did not cause any inconvenience to the subjects, and easily presented the pressure and heat stimuli (Fig. 8a and b). It was possible to present the pressure stimulation in a range from 4.5 to 8.5 psi and to keep a mostly constant level of pressure through pressure regulation (Fig. 8c). The rising time was from 0 psi to maximum pressure (8.5 psi) was 3.5 s, and the deflation time was below 0.2 s. As for the heat stimuli, although fluctuation did occur, the set baseline temperature (33 °C) and stimulation temperatures (42 °C and 49 °C) were maintained at a mostly constant level (Fig. 8d). It took approximately 7 s to rise from 33 °C to 49 °C (maximum stimulation temperature), from which the calculated temperature increase rate was approximately 2.3 °C/s. It took approximately 10 s to return from the maximum (49 °C) to the baseline temperature (33 °C), which was longer than the rising time (Fig. 8d). The temperature decrease rate calculated from the values above was approximately 1.6 °C/s.

Figure 9 shows the results of a group analysis on the pressure and heat stimulation fMRI experiments. In all activated regions, somatosensory areas are marked with white arrows. In Table 2, the MNI coordinates, regions, *t* scores, and numbers of voxels for the marked somatosensory areas are represented. When pressure stimulation was applied to the right index (Fig. 9a) and little (Fig. 9b) fingers, activation occurred in the region of the left postcentral gyrus (BA 3) and left precentral gyrus (BA4), respectively. On the other

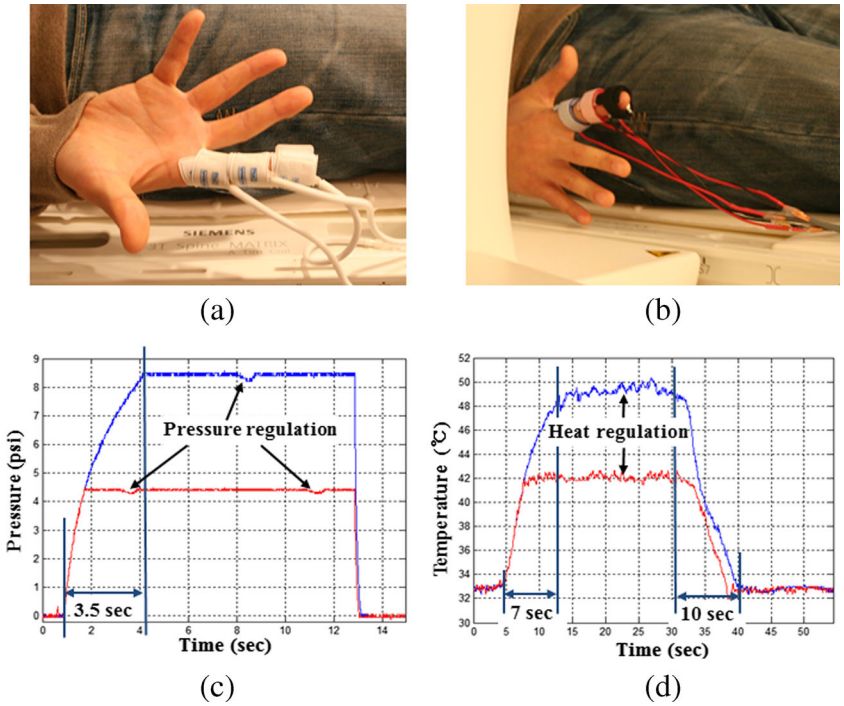

Fig. 8 Images of pressure (**a**) and heat (**b**) tactors actually put on a finger, as well as response characteristics of the pressure (**c**) and heat (**d**) tactors measured while obtaining echoplanar imaging

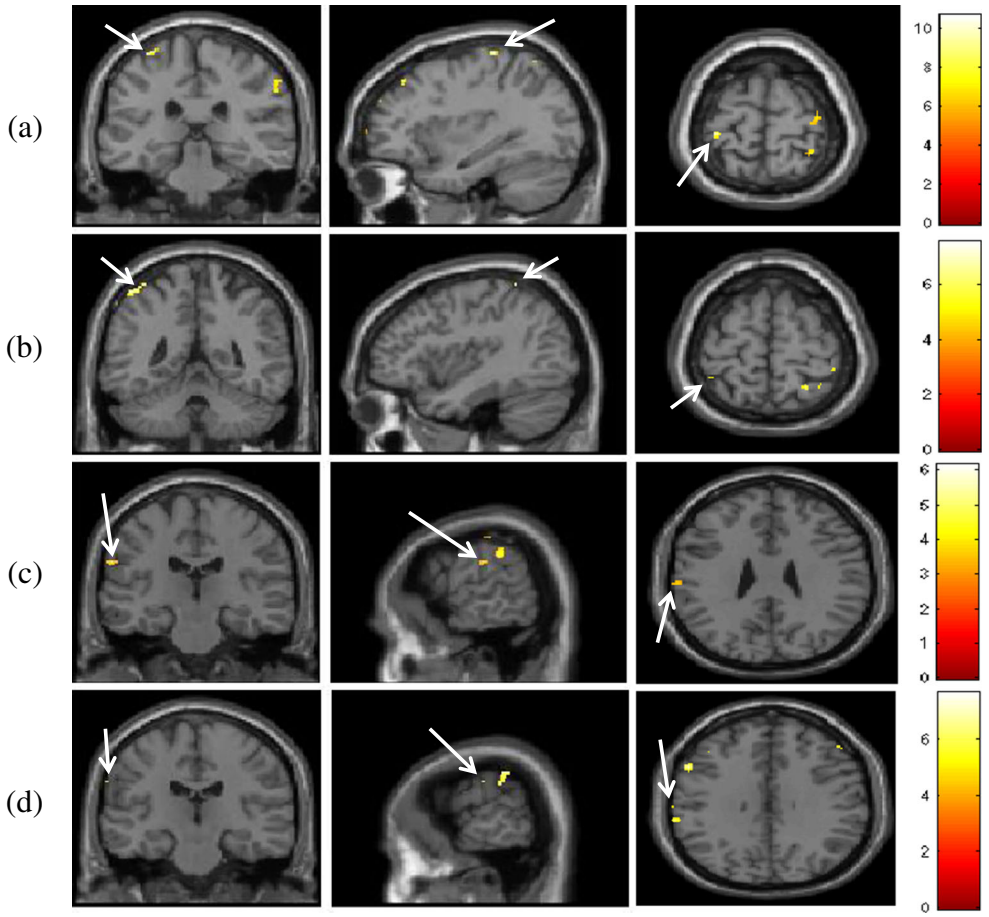

Fig. 9 Brain activation during our fMRI experiments: Brain activation regions related to pressure stimulation of the index (**a**) and little (**b**) fingers' distal phalanges, as well as regions related to heat stimulation of the index (**c**) and little (**d**) fingers' distal phalanges

hand, when heat stimulation was applied to the right index (Fig. 9c) and little (Fig. 9d) fingers, activation occurred in the region of the left postcentral gyrus (BA 2 and 1).

Discussion

This study reports a method for quantitatively controlling intra- and interdigit pressure and heat stimulation and a simple MR-compatible pressure and heat stimulator that we developed that can control stimulation variables. The stimulator can be controlled with E-Prime software, and tactile, auditory, and visual stimulation could be simultaneously generated. As compared with the existing stimulators being used in the MR environment, the developed pressure and heat stimulator has several advantages, described below.

In terms of stimulation control, the developed stimulator can precisely control stimulation intensity by using a microcontroller. With respect to the tactors, pressure tactors that make use of neonatal cuffs can apply stimulation more consistently, control the stimulation area, and present quantitatively more various intensities of stimulation than can the air-puff and diaphragm methods. In addition, our tactors offer uniform pressure stimulation to a wider area, in comparison to the von Frey filament method. In contrast with the existing Peltier Thermode, the present Peltier-element-using

Table 2 MNI coordinates, *t* scores, and numbers of voxels in regions of interest for pressure and heat stimulation on the right index and little finger

Stimulation type	Finger	Number of Voxels	*t* Score	MNI Coordinates *x*, *y*, *z* (mm)	Side	Region	Brodmann area
Pressure	Right index	28	10.68	−33 −30 70	L	Postcentral gyrus	3
	Right little	26	5.54	−39 −46 66	L	Precentral gyrus	4
Heat	Right index	19	3.83	−62 −22 28	L	Postcentral gyrus	2
	Right little	2	4.98	−65 −21 32	L	Postcentral gyrus	1

heat tactor is smaller in size and can adjust the area of stimulation. Furthermore, it can present more uniform and precise stimulation intensity to an area than is possible by using a light bulb.

In terms of the system, the developed pressure and heat stimulator simply consists of three parts: a control unit, drive units, and tactors. In particular, pressure or heat stimulation can be presented with a single system. Because it uses a rolling pump, a pressure drive unit that is very small in size can easily be installed and used, and is inexpensive to make. Furthermore, the neonatal cuff used as a pressure tactor is composed of vinyl and Velcro tape, and the heat tactors are fixed by Velcro tape, making them easy to attach and detach on intra- and interdigit areas. In summary, the stimulator developed here has some big advantages over conventional stimulators, in that it is small in size, inexpensive, and easy to install.

In the phantom experiment with three operating conditions of the heat tactors, the SNR of the EPI was almost constant and, moreover, the EPI obtained from activating the heat tactors did not show any image distortion. Also, because the pressure and heat stimulators were stable while acquiring the EPI, the developed pressure and heat stimulator was confirmed to be MR-compatible. Additionally, because of the excellent performance of the noise filter protecting the heat drive unit, the developed stimulator can be used without compensation for all MR scanners below 3.0 T.

This study presents data from pressure and heat stimulation to the distal phalanges of the right index and little fingers using the system that we developed, and it identifies differences in the activation related to different somatosensory areas. These results imply that the developed stimulator can actively be utilized to identify perceptional and cognitive characteristics of pressure and heat sense in terms of brain function.

In conclusion, as compared with those of the existing pressure and heat stimulators, the developed stimulator shows excellent improvements in terms of stimulation control, tactors, the overall system, and cost. It is expected to be utilized actively in future intra- and interdigit fMRI studies.

Author Note This research was supported by the Pioneer Research Center Program through the National Research Foundation of Korea funded by the Ministry of Science, ICT & Future Planning (Grant No. 2011-0027920).

References

Arendt-Nielsen, L., & Chen, A. C. (2003). Lasers and other thermal stimulators for activation of skin nociceptors in humans. *Clinical Neurophysiology, 33,* 259–268.

Becerra, L. R., Breiter, H. C., Stojanovic, M., Fishman, S., Edwards, A., Comite, A. R., & Borsook, D. (1999). Human brain activation under controlled thermal stimulation and habituation to noxious heat: An fMRI study. *Magnetic Resonance in Medicine, 41,* 1044–1057.

Bleton, J. P., Vidailhet, M., Bourdain, F., Ducorps, A., Schwartz, D., Delmaire, C., & Meunier, S. (2011). Somatosensory cortical remodelling after rehabilitation and clinical benefit of in writer's cramp. *Journal of Neurology, Neurosurgery, and Psychiatry, 82,* 574–577. doi:10.1136/jnnp.2009.192476

Briggs, R. W., Dy-Liacco, I., Malcolm, M. P., Lee, H., Peck, K. K., Gopinath, K. S., & Tran-Son-Tay, R. (2004). A pneumatic vibrotactile stimulation device for fMRI. *Magnetic Resonance in Medicine, 51,* 640–643.

Chakravarty, M. M., Broadbent, S., Rosa-Neto, P., Lambert, C. M., & Collins, D. L. (2009). Design, construction, and validation of an MRI-compatible vibrotactile stimulator intended for clinical use. *Journal of Neuroscience Methods, 184,* 129–135. doi:10.1016/j.jneumeth.2009.07.018

Dresel, C., Parzinger, A., Rimpau, C., Zimmer, C., Ceballos-Baumann, A. O., & Haslinger, B. (2008). A new device for tactile stimulation during fMRI. *NeuroImage, 39,* 1094–1103.

Gallasch, E., Fend, M., Rafolt, D., Nardone, R., Kunz, A., Kronbichler, M., & Golaszewski, S. (2010). Cuff-type pneumatic stimulator for studying somatosensory evoked responses with fMRI. *NeuroImage, 50,* 1067–1073. doi:10.1016/j.neuroimage.2010.01.014

Gassert, R., Yamamoto, A., Chapuis, D., Dovat, L., Bleuler, H., & Burdet, E. (2006). Actuation methods for applications in MR environments. *Concepts in Magnetic Resonance, 29B,* 191–209.

Geyer, S., Schleicher, A., Schormann, T., Mohlberg, H., Bodegard, A., Roland, P. E., & Zilles, K. (2001). Integration of microstructural and functional aspects of human somatosensory areas 3a, 3b, and 1 on the basis of a computerized brain atlas. *Anatomy and Embryology, 204,* 351–366.

Gizewski, E. R., Koeze, O., Uffmann, K., de Greiff, A., Ladd, M. E., & Forsting, M. (2005). Cerebral activation using a MR-compatible piezoelectric actuator with adjustable vibration frequencies and in vivo wave propagation control. *NeuroImage, 24,* 723–730. doi:10.1016/j.neuroimage.2004.09.015

Golaszewski, S. M., Siedentopf, C. M., Baldauf, E., Koppelstaetter, F., Eisner, W., Unterrainer, J., & Felber, S. R. (2002). Functional magnetic resonance imaging of the human sensorimotor cortex using a novel vibrotactile stimulator. *NeuroImage, 17,* 421–430.

Graham, S. J., Staines, W. R., Nelson, A., Plewes, D. B., & McIlory, W. E. (2001). New devices to deliver somatosensory stimuli during functional MRI. *Magnetic Resonance in Medicine, 46,* 436–442.

Habre-Hallage, P., Hermoye, L., Gradkowski, W., Jacobs, R., Reychler, H., & Grandin, C. B. (2010). A manually controlled new device for punctuate mechanical stimulation of teeth during functional magnetic resonance imaging studies. *Journal of Clinical Periodontology, 37,* 863–872.

Harrington, G. S., Wright, C. T., & Downs, J. H. (2000). A new vibrotactile stimulator for functional MRI. *Human Brain Mapping, 10,* 140–145.

Hegner, Y. L., Saur, R., Veit, R., Butts, R., Leiberg, S., Grodd, W., & Braun, C. (2007). BOLD adaptation in vibrotactile stimulation: Neuronal networks involved in frequency discrimination. *Journal of Neurophysiology, 97,* 264–271. doi:10.1152/jn.00617.2006

Hlushchuk, Y., Forss, N., & Gari, R. (2004). Distal-to-proximal representation of volar index finger in human area 3b. *NeuroImage, 21,* 696–700.

Hlushchuk, Y., & Hari, R. (2006). Transient suppression of ipsilateral primary somatosensory cortex during tactile finger stimulation. *Journal of Neuroscience, 26,* 5819–5824.

Ho, C., & Spence, C. (2007). Head orientation biases tactile localization. *Brain Research, 1144,* 236–241. doi:10.1016/j.brainres.2007.01.091

Huang, R. S., & Sereno, M. I. (2007). Dodecapus: An MR-compatible system for somatosensory stimulation. *NeuroImage, 34,* 1060–1073.

Kim, H. S., Yeon, H. W., Choi, M. H., Kim, J. H., Choi, J. S., Park, J. Y., & Chung, S. C. (2011). Development of a tactile stimulator with simultaneous visual and auditory stimulation using E-Prime software. *Computer Methods in Biomechanics and Biomedical Engineering, 16,* 481–487.

Kubina, B., Ristić, D., Weber, J., Stracke, C. P., Forster, C., & Ellrich, J. (2010). Bilateral brainstem activation by thermal stimulation of the face in healthy volunteers. *Journal of Neurology, 257,* 271–280. doi:10.1007/s00415-009-5307-z

Mertens, M., & Lutkenhoner, B. (2000). Efficient neuromagnetic determination of landmarks in the somatosensory cortex. *Clinical Neurophysiology, 111,* 1478–1487.

Montant, M., Romaiguère, P., & Roll, J. P. (2009). A new vibrator to stimulate muscle proprioceptors in fMRI. *Human Brain Mapping, 30,* 990–997. doi:10.1002/hbm.20568

Mottonen, R., Jarvelainen, J., Sams, M., & Hari, R. (2004). Viewing speech modulates activity in the left SI mouth cortex. *NeuroImage, 24,* 731–737.

Overduin, S. A., & Servos, P. (2004). Distributed digit somatotopy in primary somatosensory cortex. *NeuroImage, 23,* 462–472.

Peltz, E., Seifert, F., DeCol, R., Dörfler, A., Schwab, S., & Maihöfner, C. (2011). Functional connectivity of the human insular cortex during noxious and innocuous thermal stimulation. *NeuroImage, 54,* 1324–1335. doi:10.1016/j.neuroimage.2010.09.012

Roiha, K., Kiveskari, E., Kaste, M., Mustanoja, S., Makela, J. P., Salonen, O., & Forss, N. (2011). Reorganization of the primary somatosensory cortex during stroke recovery. *Clinical Neurophysiology, 122,* 339–345.

Schweisfurth, M. A., Schweizer, R., & Frahm, J. (2011). Functional MRI indicates consistent intra-digit topographic maps in the little but not the index finger within the human primary somatosensory cortex. *NeuroImage, 56,* 2138–2143.

Tsekos, N. V., Khanicheh, A., Christoforou, E., & Mavroidis, E. (2007). Magnetic resonance-compatible robotic and mechatronics systems for image-guided interventions and rehabilitation: A review study. *Annual Review of Biomedical Engineering, 9,* 351–387.

Van Westen, D., Fransson, P., Olsrud, J., Rosen, B., Lundborg, G., & Larsson, E. M. (2004). Finger somatotopy in area 3b: An fMRI-study. *BMC Neuroscience, 5,* 28.

Wienbruch, C., Candia, V., Svensson, J., Kleiser, R., & Kollias, S. S. (2006). A portable and low-cost fMRI compatible pneumatic system for the investigation of the somatosensory system in clinical and research environments. *Neuroscience Letters, 398,* 183–188.

Zhang, W. T., Jin, Z., Cui, G. H., Zhang, K. L., Zhang, L., Zeng, Y. W., & Han, J. S. (2003). Relations between brain network activation and analgesic effect induced by low vs. high frequency electrical acupoint stimulation in different subjects: A functional magnetic resonance imaging study. *Brain Research, 982,* 168–178.